Anal. Bioanal. Electrochem., Vol. 16, No. 12, 2024, 1072-1084
https://www.doi.org/10.22034/abec.2024.719409

Analytical & Bioanalytical Electrochemistry

Full Paper

Corrosion Inhibition Effect of Expired Fluticasone Propionate on API 5L Grade B Steel in A Sodium Chloride Medium

Sihem Kherraf,[1,2,*] Zohra Djetoui,[2] and Malika Foudia[3]

[1]*Laboratory of Chemical Engineering and Environment of Skikda, University of 20 August 1955-Skikda, Algeria*
[2]*Departement of Petrochemicals, Faculty of Technology, University of 20 August 1955-Skikda, Skikda, Algeria*
[3]*Laboratory of Energy and Electrochemistry of Solids, Faculty of Technology, Ferhat Abbas University Setif-1, Setif 19000, Algeria*

*Corresponding Author, Tel.: +20-6678583949
E-Mail: s.kherraf@univ-skikda.dz

Received: 17 September 2024 / Received in revised form: 4 December 2024 / Accepted: 16 December 2024 / Published online: 31 December 2024

Abstract- Fluticasone propionate, a steroid medication commonly used to treat asthma and allergic rhinitis, was evaluated for its potential as a corrosion inhibitor for API 5L Grade B steel in a 3.5% sodium chloride medium. The experimental techniques employed included the gravimetric method, potentiodynamic polarization, electrochemical impedance spectroscopy measurements, and surface analysis. The results demonstrated that fluticasone propionate is an effective corrosion inhibitor, with inhibition efficiencies of 90.10%, 91.86%, and 92.91% as determined by the weight loss method, polarization studies, and the electrochemical impedance spectroscopy technique, respectively. As the inhibitor concentration was increased in the corrosive solution, the charge transfer resistance also increased, due to the growing thickness of the electrical double layer. Polarization data indicated that the drug acted as a mixed-type inhibitor. Adsorption studies confirmed that the adsorption process was spontaneous and involved a physisorption mechanism: adsorption of the drug compounds onto the metal surface followed the Langmuir adsorption isotherm model. An increase in the electrolyte temperature led to a decrease in the inhibition efficiency from 90.10% to 72.45%. A thermodynamic analysis revealed that the addition of the inhibitor led to an increase in the activation energy of the test solution from 6.06 $kJ.mol^{-1}$ to 31.04 $kJ.mol^{-1}$, thus confirming the formation of a protective layer that reduced the kinetics of the corrosion reactions. Surface analysis revealed that the inhibited sample showed less deterioration compared to the uninhibited one.

Keywords- Corrosion; Carbon steel; Drug inhibitor; Polarization; Electrochemical impedance spectroscopy

1. INTRODUCTION

Carbon steels are essential metallic materials in industry, and are widely used in the manufacturing of pipelines for the petroleum, chemical and petrochemical sectors [1]. In petroleum refineries, steel pipelines are used to transport oil mixed with water, high-salinity formation water, or seawater; however, prolonged exposure to saline water can cause localized corrosion of the metal surface, as chloride ions promote the breakdown of the protective passive layer [2]. Möller et al. [3] reported that low-carbon steel exhibited corrosion in both natural and artificial seawaters, with the corrosion rate being nearly four times higher in a 3.5% NaCl solution compared to natural seawater. Wang et al. [4] found that X80 steel pipelines are highly vulnerable to pitting corrosion in chloride solutions with a pH range of 4 to 12.5. The corrosion of carbon steel is a major industrial problem, as it can lead to equipment failure and significant financial losses [5], and effective corrosion prevention measures are therefore essential to maintain the durability of industrial equipment .

Chemical inhibitors are among the most effective methods for controlling metal dissolution. These substances are applied in small amounts to corrosive environments, and reduce the kinetics of the corrosion reactions by forming a protective layer on the steel surface [6]. Unfortunately, many chemical inhibitors are toxic and poorly biodegradable, posing risks to both ecological environments and human health. Recently, researchers have increasingly focused on the use of pharmaceutical drugs, which have shown high inhibitory efficiency, are non-toxic, and are relatively inexpensive [7]. The effective performance of pharmaceuticals as inhibitors is attributed to the presence of active centers such as heteroatoms and aromatic groups in their structure, which adsorb onto metal surfaces, thereby inhibiting the anodic and cathodic reactions of corrosion [8].

The literature contains numerous studies on the application of expired pharmaceuticals as anti-corrosion products for carbon steel in acidic environments [9-13]; however, there is limited information regarding their anticorrosion efficiency in neutral chloride media. Sundaram et al. [14] performed a comparative investigation of the anticorrosion properties of Acarbose, Miglitol, and Voglibose on the corrosion of mild steel in a sodium chloride medium. Their results demonstrated that all of these inhibitors had a high inhibition efficiency and acted as anodic-type inhibitors. The corrosion inhibition process was due to the geometric coverage effect of these inhibitors. Abeng et al. [15] studied the effect of clonazepam on the corrosion behavior of mild steel in a 3.5% sodium chloride solution, and found that the inhibitor displayed good inhibition efficiency. The high inhibitory activity of clonazepam was linked to the formation of an adsorbed layer on the metal surface. Ebrahim et al. [16] demonstrated that hexamine is an effective inhibitor for mitigating mild steel corrosion, with an inhibition

efficiency of 92%. Macedo et al. [17] found that imidazole and its derivatives ameliorate the corrosion resistance of iron in sodium chloride solutions by acting as anodic inhibitors, while Raghavendra et al. [18] reported that the drug Ceftin provides effective protection against the dissolution of carbon steel in 3% chloride sodium solutions. In a separate study, Raghavendra et al. [19] found that the inhibitory effect of expired oxazepam in a 5% chloride sodium medium increases with increasing inhibitor content but decreases with extended contact time. Anand et al. [20] reported that tetracycline and neomycin trisulfate reduce the dissolution rate of mild steel in a 2M chloride sodium solution by 82.90% and 75.10%, respectively. Mahmoud et al. [21] demonstrated that amoxicillin effectively mitigates the corrosion of carbon steel in 0.6 M chloride sodium medium through the adsorption process .

Fluticasone propionate (FP) is an inhaled corticosteroid with anti-allergic and anti-inflammatory effects that is widely administered for the treatment of asthma and allergic rhinitis [22,23]. It consists of heteroatoms (fluorine, oxygen, sulfur), a hydroxyl group (O-H), an aromatic ring (C=C), an ether group (C-O), and a carbonyl group (C=O) (Figure 1) [24], which are key features of an effective corrosion inhibitor. Although various pharmaceutical compounds have been explored for their potential as corrosion inhibitors, there is no prior research on the use of FP for this purpose. The aim of this study is to evaluate the effectiveness of expired FP in reducing the corrosion of API 5L Grade B carbon steel in a 3.5% sodium chloride solution. The investigation was carried out using the gravimetric method, electrochemical techniques including polarization and electrochemical impedance spectroscopy, and surface characterization.

2. EXPERIMENTAL SECTION

2.1. Materials and Methods

Corrosion experiments were conducted using API 5L Grade B carbon steel specimens with the following chemical composition (wt.%): 0.086 C, 0.011 P, 0.232 Si, 0.002 S, 0.014 Cu, 0.076 N, 0.015 Al, 0.001 V, 0.001 Mo, 0.008 Ti, 1.35 Mn, 0.009 Cr, and the remainder Fe.

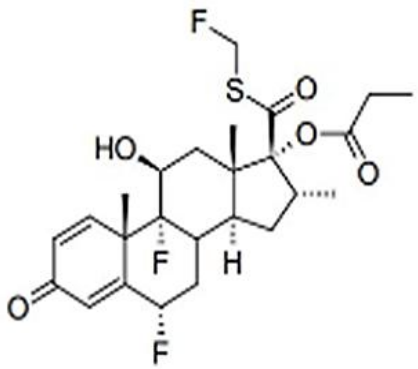

Figure 1. Chemical structure of fluticasone propionate drug [25]

Electrochemical studies were conducted using a working electrode with an exposed area of 1 cm^2, while the weight loss tests used specimens with dimensions of 20×10×4 mm. Prior to each test, the steel samples were abraded with abrasive sheets with different granulations (ranging from 240 to 1200), and were then rinsed with running water and degreased with acetone to remove any residual impurities. The test solution was prepared by dissolving 35 g of chloride sodium powder in 1 L of distilled water. All experiments were performed using different concentrations of FP, which varied from 1.3 to 5.25 g/L.

2.2. Electrochemical Measurements

Electrochemical investigations were conducted at 298 K using a potentiostat/galvanostat (Voltalab PGZ301) and a three-electrode configuration with a working electrode of API 5L Grade B carbon steel, a reference electrode of saturated calomel electrode (SCE), and a counter electrode. Potentiodynamic polarization curves were obtained at a scan rate of 1 mV/s, and electrochemical impedance spectroscopy (EIS) measurements were recorded over a frequency range from 100 kHz to 10 mHz with a sinusoidal wave excitation of ±10 mV. The inhibition efficiencies (IE_P%) and (IE_{EIS}%) were calculated using Eqs. (1) and (2) [25,26]:

$$IE_p\ \% = \frac{i^0_{corr} - i_{corr}}{i^0_{corr}} \times 100 \quad (1)$$

$$IE_{EIS}(\%) = \frac{R_{ct} - R^0_{ct}}{R_{ct}} \times 100 \quad (2)$$

where R^0_{ct} and R_{ct} represent the charge transfer resistances in the absence and presence of different concentrations of FP, respectively; and i^0_{corr} and i_{corr} refer to the density of the corrosion current of carbon steel in uninhibited and inhibited media, respectively.

2.3. Gravimetric analysis

Polished and dried specimens were weighed with an electronic balance and dropped into test solutions for 24 h at different temperatures (298–333 K). After the soaking process, the metal samples were removed from the corrosive electrolytes, rinsed with acetone and distilled water, and then dried and weighed. Eqs. (3) and (4) [27] were used to calculate the corrosion rate (C_R) for carbon steel specimens and the inhibition efficiency (IE_{WL}%) based on the average weight loss.

$$C_R = \Delta W / S.t \quad (3)$$

$$IE_{WL}\ (\%) = \frac{C^0_R - C_R}{C^0_R} \times 100 \quad (4)$$

where ΔW is the weight loss of the metal surface, S represents the exposed area of the specimen, t is the duration of exposure, and C^0_R and C_R represent the corrosion rates of the specimens in uninhibited and inhibited solutions, respectively.

2.4. Surface Morphology

The surface morphology of the steel samples was examined using optical microscopy after immersion in either uninhibited and inhibited solutions for 24 h.

3. RESULTS AND DISCUSSION

3.1. Polarization study

Polarization measurements were performed to investigate the kinetics of the anodic and cathodic reactions occurring at the electrical double layer. The influence of increasing the FT concentration on the corrosion rate of API 5L Grade B steel in the corrosive electrolyte is depicted in the Tafel plots in Figure 2. The anodic domain is associated with the oxidation of iron atoms (Eq. (5)), while the cathodic branch is linked to the reduction of oxygen (Eq. (6)) [28].

$$Fe \rightarrow Fe^{2+} + 2é \quad (5)$$

$$O_2 + 2H_2O + 2é \rightarrow 4OH^- \quad (6)$$

As shown in Figure 2, the shapes of the polarization plots for inhibited solutions do not differ significantly from that of the inhibitor-free NaCl solution. This suggests that the inhibitor ameliorates the corrosion resistance of the carbon steel without affecting the electrochemical mechanisms.

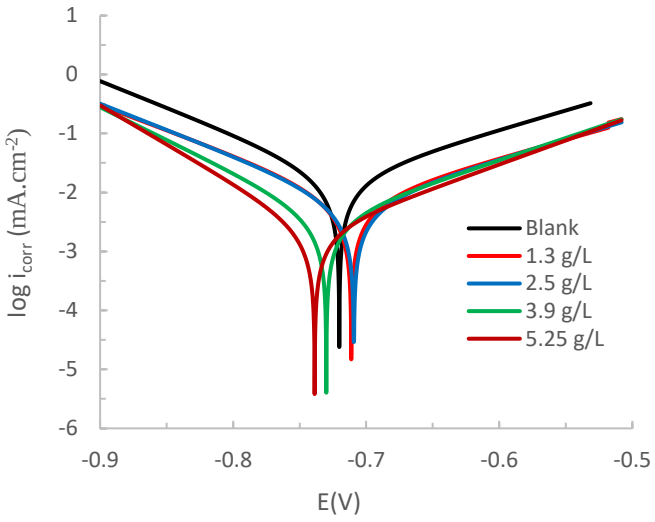

Figure 2. Polarization curves of API 5L Grade B steel immersed in 3.5% sodium chloride solution containing different concentrations of FP at 298 K

The kinetic parameters, including Tafel slopes for both cathodic (βc) and anodic (βa) reactions, corrosion potential (E_{corr}), corrosion current density (i_{corr}), and inhibition efficiency (IE_{pol} %), are presented in Table 1.

The recorded results show that the introduction of the drug FP at various concentrations to the test solution led to decreases in the corrosion current density from 26.91 to 2.19 ($\mu A.cm^{-2}$). The corrosion inhibition effect can be attributed to the formation of a protective film which blocks the active sites on the metal surface. It should also be noted that the presence of FP in the corrosive electrolyte shifted the corrosion potential by 525 mV compared to that of the blank, indicating that the inhibitor can be characterized as a mixed inhibitor [29,30].

Table 1. Polarization parameters for carbone steel in both blank and inhibited solutions

C_{inh} ($g.L^{-1}$)	E_{corr} (mV)	i_{corr} ($\mu A.cm^{-2}$)	β_a ($mV.dec^{-1}$)	β_c ($mV.dec^{-1}$)	IE_{pol} (%)
Blank	-720.21	26.91	152.6	111.8	-
1.3	-711.19	7.55	149.3	110	71.94
2.5	-709.21	5.35	142.2	104	80.11
3.9	-729.93	3.85	132.4	90.4	85.69
5.25	-738.71	2.19	122.6	75.6	91.86

3.2. Electrochemical impedance spectroscopy measurements

Figures 3(a) and (b) present Nyquist and Bode plots, which were measured for the corroding steel electrode in a 3.5% NaCl electrolyte with and without various concentrations of the inhibitor. The figure indicates that the impedance spectra for carbon steel in the uninhibited solution have a single relaxation time constant, suggesting that the corrosion process is controlled by a charge transfer mechanism [15]. The equivalent electrical circuit depicted in Fig. 4(a) was employed to model the API 5L Grade B/solution interface. Since the impedance diagrams took the form of depressed semicircles, a constant phase element (CPE) was used to represent the non-ideal capacitive response. In the circuit, R_s and R_{ct} represent the electrolyte resistance and the charge transfer resistance, respectively, and CPE_{dl} corresponds to the constant phase element characterizing the double layer capacitance. The impedance of the CPE was calculated using Eq. (7) [31]:

$$Z_{CPE} = Q_0^{-1}(j\omega)^{-n} \qquad (7)$$

where Q_0 denotes the modulus of the CPE; ω represents the angular frequency; j is the imaginary number; and n is a measure of surface irregularity ($0 < n < 1$).

In the presence of the inhibitor, two capacitive loops are necessary for fitting of the impedance results. The corresponding equivalent circuit shown in Figure 4(b) includes an additional R_f-CPE_f couple that is located in the high frequency region, and this can be ascribed to the formation of a protective film. The resistance and the capacitance of this protective barrier are represented by R_f and CPE_f, respectively. The values of the fitting parameters and the inhibition efficiency ($\%IE_{EIS}$) are given in Table 2, and it is clear that there is a noticeable

increase in R_{ct} and R_f values as the concentration of the inhibitor rises, whereas the Q_{dl} and Q_f values decrease.

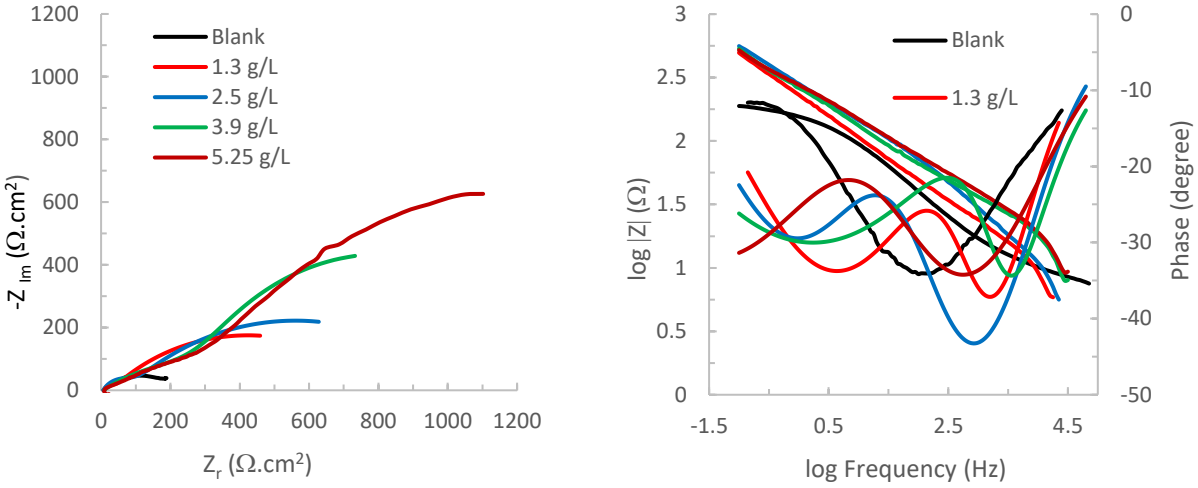

Figure 3. Electrochemical impedance diagrams of API 5L Grade B steel in the corrosive medium containing different concentrations of the inhibitor at 298K (a) Nyquist diagrams and (b) Bode plots

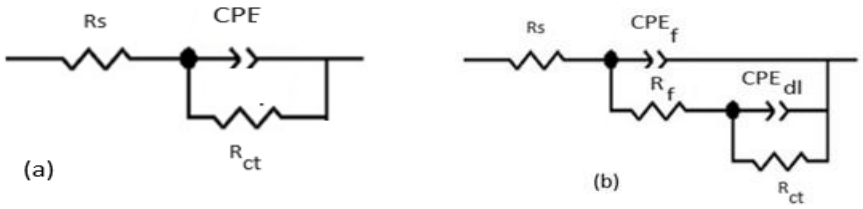

Figure 4. Equivalent circuit used to model the metal/electrolyte interface

Table 2. EIS parameters for API 5L Grade B steel immersed in 3.5% sodium chloride medium containing different doses of inhibitor at 298 K

		CPE$_f$			**CPE$_{dl}$**			
C_{inh} **(g.L^{-1})**	**R_s** **(Ω.cm^2)**	**Q_f** **(mF.cm^{-2})**	**n_f**	**R_f** **(Ω.cm^2)**	**Q_{dl}** **(mF.cm^{-2})**	**n_{dl}**	**R_{tc}** **(Ω.cm^2)**	**IE_{EIS}** **(%)**
Blank	6,975				1,46	0,61	212,9	
1.3	7,14	1,261	0,66	22,36	1,168	0,63	788,7	73
2.5	6,417	1,014	0,75	220,6	1.08	0,71	1 127	81.18
3.9	6,471	0,809	0.80	420,8	0,927	0,85	1 606	86.74
5.25	6,277	0,514	0,90	697,7	0,513	0,89	2 769	92.91

The most significant effect was observed at an inhibitor concentration of 5.25 g/L, which gives a value for $\%IE_{EIS}$ of 92.91%. The increase in R_{ct} and R_f values is due to the formation of a protective coating on the electrode surface, which creates a resistive effect that delays the charge transfer process between the metal surface and the electrolyte interface. In addition, the decrease in Q_{dl} and Q_f values is related to the reduction in the local dielectric constant as the thickness of the electrical double layer increases [32,33].

3.3. Adsorption mechanism

The inhibitory effect of organic inhibitors depends mainly on their ability to adsorb onto the metal surface. The adsorption process can be considered a substitution reaction between the inhibitor molecules in the aqueous phase and the water molecules that have already been adsorbed, as described by the following reaction [34]:

$$FP_{(sol)} + xH_2O_{(ads)} \rightleftharpoons FP_{(ads)} + xH_2O_{(sol)} \quad (8)$$

where $FP_{(sol)}$ and $FP_{(ads)}$ represent the inhibitor dissolved in a 3.5%NaCl solution and the inhibitor adsorbed onto the metal surface, respectively. Similarly, $H_2O_{(sol)}$ and $H_2O_{(ads)}$ represent the water molecules in the electrolyte and those adsorbed onto the metal surface, respectively. The variable x denotes the number of water molecules substituted by one molecule of the inhibitor.

To understand the nature of the interactions between the inhibitor molecules and the active sites on the metal surface, data obtained with the electrochemical impedance spectroscopy technique were fitted to various adsorption isotherms, including the Langmuir, Temkin, Freundlich, Frumkin, and Flory–Huggins isotherms. The results indicated that the Langmuir isotherm, as expressed in Eq. (9) [35], provided the best fit, with a regression coefficient of approximately 0.998. This suggests that the drug constituents are efficiently adsorbed onto the steel surface as a monolayer [36].

$$\frac{C_{inh}}{\theta} = \frac{1}{K_{ads}} + C_{inh} \quad (9)$$

where C_{inh} is the concentration of the drug FP; K_{ads} is the equilibrium constant of the adsorption process; and θ is the surface coverage of exposed carbon steel, which is calculated based on the charge transfer resistance values using Eq. (10):

$$\theta = \frac{R_{ct} - R_{ct}^0}{R_{ct}} \quad (10)$$

The standard free energy of adsorption (ΔG_{ads}^0) provides valuable insights into the nature of the adsorption process. The values of ΔG_{ads}^0 are determined using Eq. (11) [37,38]:

$$\Delta G_{ads}^0 = -RT \ln (10^3 K_{ads}) \quad (11)$$

where T is the electrolyte temperature; R is the gas constant; and 10^3 represents the concentration of water in the solution expressed in $g.L^{-1}$. It has been reported that a value for

ΔG^0_{ads} of close to −20 kJ. mol^{-1} (or less negative) suggests physisorption, whereas a ΔG^0_{ads} value of approximately −40 kJ.mol^{-1} (or more negative) indicates chemisorption [39]. In this study, the calculated ΔG^0_{ads} value was −4.45 kJ. mol^{-1}; this is less negative than −20 kJ. mol^{-1}, indicating that the drug molecules interact with the steel surface through electrostatic binding (physical adsorption) and form a film barrier that inhibits the corrosion process. The negative sign for the ΔG^0_{ads} value confirms that the adsorption of the inhibitor compounds onto the metal surface is spontaneous.

3.4. Temperature effect

Table 3 presents the values for the corrosion rates of API 5L Grade B steel at temperatures ranging from 298 K to 328 K in both uninhibited and inhibited solutions. The results indicate that the corrosion rate of the steel surface gradually decreases as the inhibitor concentration is increased across the entire temperature range examined here. This phenomenon is attributed to the increased number of adsorbed molecules on the electrode surface, which block the active sites and thereby protect the metal from corrosion [40]. Furthermore, the inhibition efficiency decreases from 90.10% to 72.45% as the temperature rises from 298 K to 328 K. This behavior is likely to be due to the enhanced rate of desorption of the drug constituents from the steel surface [41,42].

To gain a better understanding of the effect of temperature, various parameters, including the activation energy (E_a), activation entropy (ΔS_a), and activation enthalpy (ΔH_a), were calculated using the Arrhenius equation (Eq. (12)) and the transition state equation (Eq. (13)) [43].

$$C_R = A\, e\, (-\frac{E_a}{RT}) \quad (12)$$

$$C_R = \frac{RT}{Nh}\, e\left(\frac{-\Delta S_a}{R}\right) e\,(\frac{-\Delta H_a}{RT}) \quad (13)$$

Where A represents the Arrhenius factor, h is Plank's constant, and N represents Avogadro's number. The values of E_a could be calculated from the slope of the Arrhenius plots (Figure 5(a)), while ΔH_a and ΔS_a were determined from the slope and intercept of the Arrhenius transition plots (Figure 5(b)). The activation energy of the blank solution ranged from 6.06 kJ.mol^{-1} to 31.04 kJ.mol^{-1} with the addition of 5.25 g.L^{-1} of inhibitor. The increase in the activation energy of the inhibited samples signified the formation of a more protective film [44]. The activation enthalpy value followed a similar trend, increasing from 3.20 kJ.mol^{-1} for the uninhibited sample to 28.63 kJ.mol^{-1} for the solution containing 5.25 g.L^{-1} of inhibitor. Furthermore, the addition of inhibitor to the corrosive electrolyte shifted the activation entropy value of the blank solution from −344.42 J.mol^{-1}K^{-1} to values of −305.94, −285.14, −285.65, and −295.27 J.mol^{-1}K^{-1} in the presence of inhibitor concentrations of 1.3, 2.5, 3.9, and 5.25 g.L^{-1}, respectively. The shift in the ΔS_a value towards less negative values suggests an increase in the order as the reactants transition into the activated complex.

Table 3. Corrosion rates and inhibition efficiencies obtained from weight loss method for carbon steel in 3.5% sodium chloride solutions free and containing different PF concentrations at different temperatures

C_{inh} (g.L^{-1})	Temperature (K)							
	298		308		318		328	
	$C_R.10^3$ (mg.cm^{-2}h^{-1})	IE_G (%)	$C_R.10^3$ (mg.cm^{-2}h^{-1})	IE_G (%)	$C_R.10^3$ (mg.cm^{-2}h^{-1})	IE_G (%)	$C_R.10^3$ (mg.cm^{-2}h^{-1})	IE_G (%)
Blank	1.596		1.76		1.853		2	
1.3	0.430	73	0.767	56.42	0.799	56.88	0.869	56.55
2.5	0.250	84.33	0.532	69.77	0.641	65.40	0.732	63.4
3.9	0.188	88.22	0.513	70.85	0.532	71.28	0.581	70.95
5.25	0.158	90.10	0.483	72.55	0.502	72.90	0.551	72.45

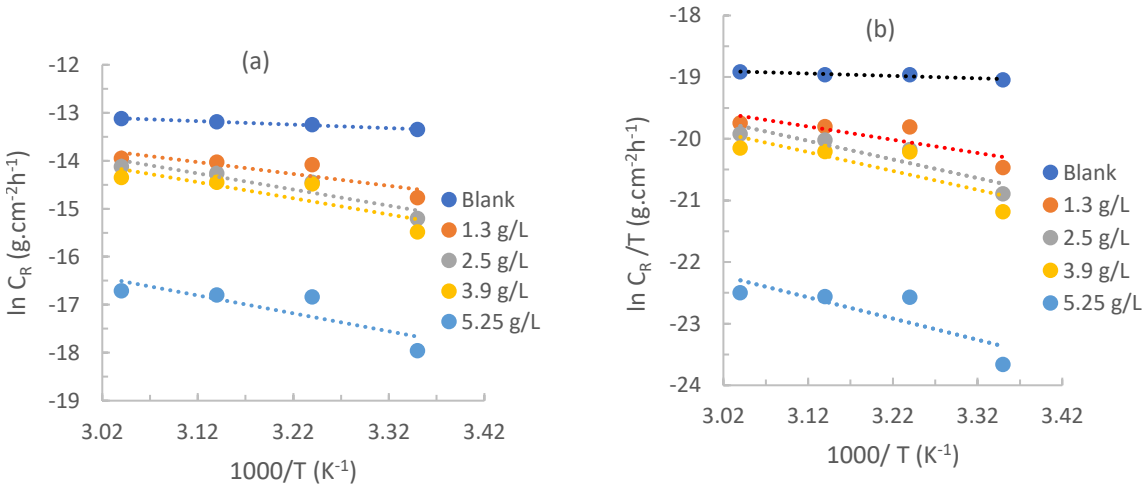

Figure 5. (a) Arrhenius and (b) transition states diagrams of FP at various temperatures

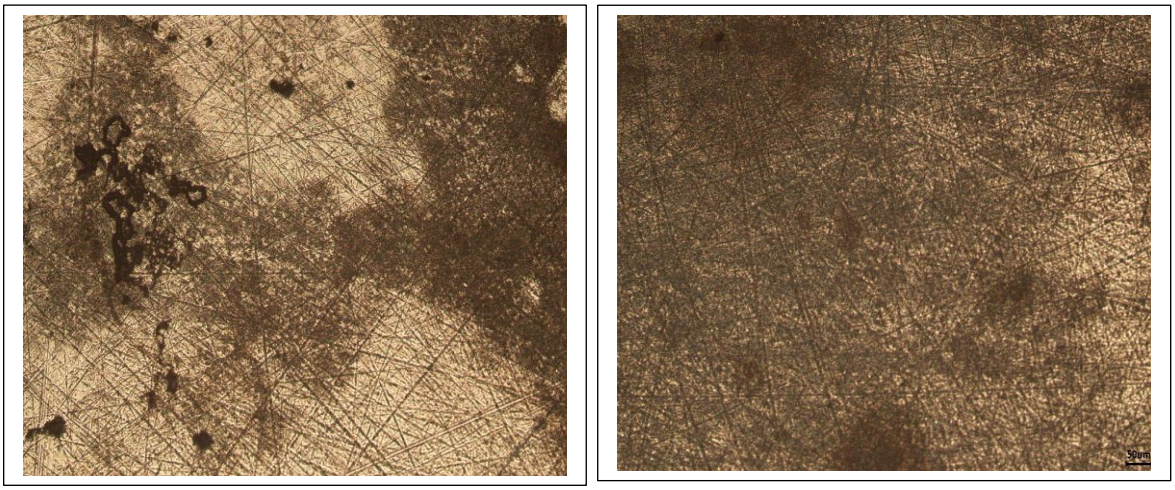

Figure 6. Optical images of (a) unprotected and (b) inhibited samples after 24 hours of immersion in the corrosive solutions

3.5. Surface investigation

Figures 6(a) and (b) show the surface morphology of API 5L Grade B steel after 24 h of exposure to the test electrolyte, both without and with 5.25 g/L of expired FP. Figure 6(a) shows that the surface of the unprotected steel sample is strongly corroded, with cracks and pits. In contrast, Figure 6(b) reveals that the inhibited sample has a smooth surface with less morphological damage compared to the non-inhibited sample. The improvement in surface morphology is due to the formation of a protective film by FP molecules over the API 5L Grade B steel, which mitigates the corrosion process.

4. CONCLUSION

The inhibition performance of expired FP against the corrosion of API 5L Grade B steel in a sodium chloride solution at different temperatures was investigated using electrochemical measurements, the gravimetric method, and surface characterization. The results indicated that the corrosion rate of API 5L Grade B steel was reduced with increasing FP content. The lowest corrosion rate was observed for the solution containing 5.25 $g.L^{-1}$ of inhibitor. The addition of the inhibitor to the test solution led to a decrease in the corrosion current density and an increase in the charge transfer resistance of the electrical double layer, indicating an increase in the corrosion resistance of carbon steel. The polarization curves revealed that the drug FP acted as a mixed-type inhibitor. The adsorption of the inhibitor onto the steel surface followed the Langmuir adsorption isotherm, and the free energy of adsorption revealed a spontaneous process, with a physisorption mechanism. An increase in the electrolyte temperature decreased the protective effect of the inhibitor due to a shift in the adsorption/desorption equilibrium of FP towards desorption. A surface analysis showed that the dissolution of the steel was greatly mitigated by the adsorption of the inhibitor compounds onto the electrode surface.

Declarations of interest

The authors declare no conflict of interest in this reported work.

REFERENCES

[1] F.E. Abeng, and V.C. Anadebe, Comput. Theor. Chem. 1229 (2023) 114334.

[2] N. Palaniappan, J. Alphonsa, I.S. Cole, K. Balasubramanian, and I.G. Bosco, Mater. Sci. Eng. B 249 (2019) 114423.

[3] H. Mölle, E.T. Boshoff, and H. Froneman, J. South. Afr. Inst. Min. Metall. 106 (2006) 585.

[4] Y. Wang, G. Cheng, W. Wu, Q. Qiao, Y. Li, and X. Li, Appl. Surf. Sci. 349 (2015) 746.

[5] K. Dahmani, M. Galai, M. Rbaa, A. Ech-Chebab, N. Errahmany, L. Guo, A.A. AlObaid, A. Hmada, I. Warad, M.E. Touhami, and M. Cherkaoui, J. Mol. Struct. 1295 (2024) 136514.
[6] S. Shojaee, M.S. Zandi, and N. Rastakhiz. J. Indian Chem. Soc. 99 (2022) 100700.
[7] M. Alfakeer, M. Abdallah, and A. Fawzy, Int. J. Electrochem. Sci. 15 (2020) 3283.
[8] M.S. Bejandi, M.H. Behroozi, M.R. Khalili, R. Sharifi, A.A. Javidparvar, and E. Oguzie, J. Industrial Eng. Chem. 131 (2024) 662.
[9] I. Ahamad, R. Prasad, and M. A. Quraishi, Corros. Sci. 52 (2010) 3033-3041.
[10] S.K. Shukla, A.K. Singh, I. Ahamad, and M.A. Quraishi, Mater. Lett. 63 (2009) 819.
[11] A.I. Ikeuba, F.O. Faithpraise, K.I. Nwokolo, F.E. Umo, O.C. Echem, A.T. Ibrahim, H. Edet, B.I. Ita, P.C. Okafor, F.C. Asogwa, and J. Amajama, Results Mater. 21 (2024) 100542.
[12] S. Pour-Ali, and S. Hejazi. J. Mol. Liq. 354 (2022) 118886.
[13] H. Tajabadipour, H. Mohammadi-Manesh, and M. Shahidi-Zandi, J. Indian Chem. Soc. 99 (2022) 100285.
[14] R.G. Sundaram, G. Vengatesh, and M. Sundaravadivelu, Surf. Interfaces. 22 (2021) 100841.
[15] F.E. Abeng, B.I. Ita, V.C. Anadebe, V.I. Chukwuike, K.M. Etiowo, P.Y. Nkom, O.O. Ekerenam, N.B. Iroha, and I.J. Ikot, Results Eng. 17 (2023) 100924.
[16] F.H. Ebrahim, and M. Ghorbani, Mater. Prot. 64 (2023) 134.
[17] M.C.S.S. Macedo, O.E. Barcia, E.C. Da Silva, J.D.O. Mendes, and O.R. Mattos, J. Electrochem. Soc.159 (2012) C160.
[18] N. Raghavendra, Iranica Journal of Energy & Environment 9 (2018) 295.
[19] N. Raghavendra, Frontiers in Chemical Res. 1 (2019) 1.
[20] B. Anand, and S. Chitra, Communication in Physical Sci. 5 (2020) 1.
[21] Z.S. Mahmoud, A.K. Shams, and T.A. Salman, Baghdad Sci. J. 19 (2022) 0121.
[22] T. Tokumura, N. Yoshida, K. Mori-Yasumoto, O. Shirota, and T. Kurita, J. Pharm. Anal. 7 (2017) 297.
[23] L. Anitha, and D.P. Beda, Green Anal. Chem. 11 (2024) 100160.
[24] V.P. Musale, S.C. Jagdale, and P. Shah, Int. J. Pharm. Sci. Rev. Res. 49 (2018) 53.
[25] N. Xu, X.B. Yang, and Q.H. Zhang, J. Mol. Liq. 393 (2024) 123602.
[26] K.C.D.S. de Lima, V.M. Paiva, M.G.A. Schwarz, N.M.B. Barreto, D. Perrone, and E. D'Elia, Sustain. Chem. Pharm. 35 (2023) 101174.
[27] M.G. Dogbe, A.Y. Mafilaza, C.V. Eleutério, H. Cabral-Marques, S. Simões, and M.M. Gaspar, Pharmaceut. 11 (2019) 521.
[28] S. Mandal, S. Bej, and P. Banerjee, J. Mol. Liq. 381 (2023) 121789.
[29] S.A. Raji, A.P.I. Popoola, and O.L. Akanji, J. Mol. Struct. 1312 (2024) 138414.
[30] K.H. Rashid, and A.A. Khadom, J. Mol. Liq. 319 (2020) 114326.

[31] N. Boutaoui, M. Acila, H. Boulahbel, B. Achouri, L. Zaiter, F. Benayache, S. Benayache, I. D'Agostino, C. Campestre, and M. Locatelli, Anal. Bioanal. Electrochem. 15 (2023) 938.
[32] L. Huang, W. Liu, J. Shen, and Q. Liao, Thin Solid Films 782 (2023) 140005.
[33] B.T.D. My, D. Tuan, and D. Q. Huong, J. Mol. Struct. 1296 (2024) 136905.
[34] C. Merimi, B. Hammouti, K. Zaidi, B. Hafez, H. Elmsellem, R. Touzani, and S. Kaya, J. Mol. Struct. 1278 (2023) 134883.
[35] J. Zhang, F. Zhan, and N. Ai-Zaqri, Int. J. Electrochem. Sci. 18 (2023) 100267.
[36] A. Addoun, S. Bouyegh, M. Dahmane, O. Ferroukhi, and M. Trari, Mater. Today Commun. 21 (2019) 100720.
[37] X. Liu, Y. Gao, J. Guan, Q. Zhang, Y. Lin, C. Shi, Y. Wang, J. Du, and N. Ma, Arab. J. Chem. 16 (2023) 105066.
[38] J. Wang, L. Cui, B. Chen, X. Chen, Z. Lv, D. Chen, Y. Qiang, and T. Xiang, J. Mater. Res. Technol. 26 (2023) 6689.
[39] B. L. Lin, X. X. Zhou, T. H. Duan, C. Zhao, J. H. Zhu, and Y. Y. Xu, Arab. J. Chem. 17 (2024) 105410.
[40] M. M. Motawea, Int. J. Electrochem. Sci. 14 (2019) 6682.
[41] A. Ziouani, S. Atia, H. Hamani, T. Douadi, M. Al-Noaimi, and N. Gherraf, J. Indian Chem. Soc. 100 (2023)100832.
[42] A. El-Asri, M.M. Rguiti, A. Jmiai, R. Oukhrib, H. Bourzi, Y. Lin, and S. El Issami, J. Taiwan Inst. Chem. Eng. 142 (2023) 104633.
[43] K. H. Rashid, A.A. Khadom, S.H. Abbas, K.F. Al-azawi, and H.B. Mahood, Results Surf. Interfaces. 13 (2023) 100165.
[44] A.J. Rani, T. Sreelakshmi, and A. Joseph, J. Mol. Liq. 366 (2022) 120211.